

Unsupervised dynamic modeling of medical image transformation

Niklas Gunnarsson^{1,2}[0000–0002–9013–949X], Jens Sjölund²[0000–0002–9099–3522],
 Peter Kimstrand²[0000–0001–9667–5595], and
 Thomas B. Schön¹[0000–0001–5183–234X]

¹ Department of Information Technology, Uppsala University, Sweden

{firstname}.{surname}@it.uu.se

² Elekta Instrument AB, Stockholm, Sweden

{firstname}.{surname}@elekta.com

Please cite this version:

Niklas Gunnarsson et al. “Unsupervised dynamic modeling of medical image transformations”. In: *2022 25th International Conference on Information Fusion (FUSION)*. IEEE. 2022, pp. 01–07

```
@inproceedings{gunnarsson2022unsupervised,
  title={Unsupervised dynamic modeling of medical
  image transformations},
  author={Gunnarsson, Niklas and Sjölund, Jens
  and Kimstrand, Peter and Schön, Thomas B},
  booktitle={2022 25th International Conference on
  Information Fusion (FUSION)},
  pages={01–07},
  year={2022},
  organization={IEEE}
}
```

Unsupervised dynamic modeling of medical image transformations

Niklas Gunnarsson^{1,2}[0000–0002–9013–949X], Jens Sjölund²[0000–0002–9099–3522],
Peter Kimstrand²[0000–0001–9667–5595], and
Thomas B. Schön¹[0000–0001–5183–234X]

¹ Department of Information Technology, Uppsala University, Sweden

`{firstname}.{surname}@it.uu.se`

² Elekta Instrument AB, Stockholm, Sweden

`{firstname}.{surname}@elekta.com`

Abstract. Spatiotemporal imaging has applications in e.g. cardiac diagnostics, surgical guidance, and radiotherapy monitoring. In this paper, we explain the temporal motion by identifying the underlying dynamics, only based on the sequential images. Our dynamical model maps the inputs of observed high-dimensional sequential images to a low-dimensional latent space wherein a linear relationship between a hidden state process and the lower-dimensional representation of the inputs holds. For this, we use a conditional variational auto-encoder (CVAE) to nonlinearly map the higher-dimensional image to a lower-dimensional space, wherein we model the dynamics with a linear Gaussian state-space model (LG-SSM). The model, a modified version of the Kalman variational auto-encoder, is end-to-end trainable, and the weights, both in the CVAE and LG-SSM, are simultaneously updated by maximizing the evidence lower bound of the marginal likelihood. In contrast to the original model, we explain the motion with a spatial transformation from one image to another. This results in sharper reconstructions and the possibility of transferring auxiliary information, such as segmentation, through the image sequence. Our experiments, on cardiac ultrasound time series, show that the dynamic model outperforms traditional image registration in execution time, to a similar performance. Further, our model offers the possibility to impute and extrapolate for missing samples.

Keywords— Dynamic system, State-space models, Deep learning, Generative models, Sequential modeling, Image registration.

1 Introduction

Today, most medical imaging modalities support some form of time-resolved imaging. In some modalities, like ultrasound, it is the default mode of operation, while in others it is known under different names depending on the application, e.g. fluoroscopy [40], 4DCT [32] and 4D flow MRI [27]. It is used for analysis, in e.g. cardiac diagnostics [1] and for guidance, monitoring and control in e.g.

interventional and intraoperative percutaneous procedures and surgeries [5, 41] and image-guided radiation therapy [30, 36].

In this paper, we want to uncover the dynamics in a medical image time series based on nothing but the images themselves. Our aim is to learn a fast, nearly real-time, parameterized function, h , such that the image y_t at time t is described by the dynamical system

$$y_t = h(y_{1:t-1}) + \epsilon_t, \quad (1)$$

where $y_{1:t-1} = \{y_1, \dots, y_{t-1}\}$ are the previously observed images and ϵ_t is noise. This representation makes it possible to predict $\hat{y}_t = h(y_{1:k})$ based on observations up to time k , i.e. to impute ($t < k$), filter ($t = k$), or extrapolate ($t > k$) images. Instead of reconstructing image y_t directly from (1) we model the motion of the dynamics, i.e. the spatial transformation φ_t from a predefined reference image y . The reconstructed image is then acquired by transforming y with the spatial transformation, $y_t = y \circ \varphi_t$. Modeling the image transformations instead of the images directly enables transferring auxiliary information, such as segmentation, from one image domain to another.

Prediction of 2D video sequences has lately shown impressive results [39, 35, 14] in computer vision. Video prediction methods are usually evaluated based on the visualization of the predicted frames. Here, and in the medical domain, we are interested in explaining the true spatial transformation that generates the dynamical motion.

Temporal medical images contain high-dimensional data where the dynamics, due to cyclic and deformable motion, is nonlinear. While the linear assumption is preferable for several reasons, including tractable filtering and smoothing posteriors, it is inappropriate for the raw image series. The idea of this paper is to reduce the high-dimensional data to a low-dimensional latent space wherein the linearity assumptions are valid. For this we combine techniques from generative and dynamic modeling and train the model end-to-end. In the literature, this is referred to as a deep state-space model (DSSM) [10, 19, 25].

In the medical domain, there are many examples of motion modeling based on motion proxies [29, 38] such as tracking implanted markers using X-ray imaging or surface tracking. Those methods are limited to the accuracy and applicability of the motion proxy. To the best of our knowledge, the only example where the motion model is based directly and exclusively on the temporal medical images under study is the recent work by [23]. They model the dynamics in a low-dimensional probabilistic space using a temporal convolutional network [2] and a Gaussian process prior. In their model, the prediction length is restricted based on the motion matrix. We overcome this by modeling the dynamics as a first-order Markov process.

2 Background

The Kalman variational auto-encoder (Kalman VAE) [10] is an unsupervised model for high-dimensional sequential data that, most likely, undergoes nonlinear

dynamics. Higher-dimensional observed images, $\mathbf{y} = \{y_t\}_{t=1}^T$ are non-linearly embedded into a lower-dimensional space using a variational auto-encoder. The dynamics of the lower-dimensional features, $\mathbf{x} = \{x_t\}_{t=1}^T$ is modeled with a linear Gaussian state-space model based on a state-space process $\mathbf{z} = \{z_t\}_{t=1}^T$. Below we explain the variational auto-encoder and the linear Gaussian state-space model, and then how those are combined into the framework of Kalman VAE.

2.1 Variational auto-encoder

Similar to traditional auto-encoders [22], variational auto-encoders (VAEs) embed the input y in a lower-dimensional latent space x using an encoder, E_ϕ and reconstruct the original input with a decoder, D_θ . They differ in that VAEs are generative and reconstruct the data distribution $p_\theta(y)$ instead of a single sample y . In this case the true posterior $p_\theta(x | y)$ is intractable. By approximating the variational posterior as a multivariate Gaussian, $q_\phi(x | y) = \mathcal{N}(x | \mu^{\text{enc}}, \Sigma^{\text{enc}})$, where μ^{enc} and Σ^{enc} are the outputs from the encoder, it is possible to sample from the variational approximation. From the KL divergence between the approximate and the true posterior we can obtain a lower bound on the true likelihood

$$\log p_\theta(y) \geq \mathbb{E}_{q_\phi(x|y)} \left[\log p_\theta(y | x) + \log \frac{p_\theta(x)}{q_\phi(x | y)} \right], \quad (2)$$

where the prior over the latent space is usually chosen to be a multivariate Gaussian $p_\theta(x) = \mathcal{N}(x | 0, \mathbf{I})$. This lower bound is called the evidence lower bound (ELBO) and can be estimated by sampling [21].

2.2 Linear Gaussian state-space model

In a VAE, each sample, $x_t \in \mathbb{R}^L$, from the approximate posterior is normally distributed with mean, μ_t^{enc} , and covariance Σ_t^{enc} . If we assume Gaussian noise, it follows that the state-space vector, z_t , in our linear state-space model also follows a normal distribution. More precisely, we have a linear Gaussian state-space model (LG-SSM),

$$\begin{aligned} p(z_t | z_{t-1}) &= \mathcal{N}(z_t | Az_{t-1}, Q), \\ p(x_t | z_t) &= \mathcal{N}(x_t | Cz_t, R), \end{aligned} \quad (3)$$

where Q and R are covariance matrices for the process and measurement noise, respectively. Given an initial guess $z_1 \sim \mathcal{N}(z_1 | \mu_1, P_1)$, the joint probability distribution can be expressed using the LG-SSM model (from (3)),

$$p(\mathbf{x}, \mathbf{z}) = p(\mathbf{x} | \mathbf{z})p(\mathbf{z}) = p(z_1) \prod_{t=1}^T p(x_t | z_t) \prod_{t=2}^T p(z_t | z_{t-1}). \quad (4)$$

Given observations \mathbf{x} the mean and covariance of the state-space variables is analytically tractable using a Kalman filter [18], $\mu_{t|t}$, $P_{t|t}$, and a Rauch-Tung-Striebel (RTS) smoother [33], $\mu_{t|T}$, $P_{t|T}$.

2.3 Kalman variational auto-encoder

In the Kalman VAE a VAE is used to reduce the dimension of the image time series distribution wherein the dynamics are represented linearly using an LG-SSM in the latent space. The goal is to describe the dynamics of the system in the latent space with an LG-SSM and use the decoder to reconstruct the image time series.

Similar to a regular VAE, the ELBO can be derived from the KL divergence between the approximate and true posterior. In a Kalman VAE the approximate posterior is given by

$$q_{\phi,\gamma}(\mathbf{x}, \mathbf{z} \mid \mathbf{y}) = p_{\gamma}(\mathbf{z} \mid \mathbf{x})q_{\phi}(\mathbf{x} \mid \mathbf{y}), \quad (5)$$

and the true posterior is proportional to

$$p_{\theta,\gamma}(\mathbf{x}, \mathbf{z}, \mathbf{y}) \propto p_{\theta}(\mathbf{y} \mid \mathbf{x})p_{\gamma}(\mathbf{x}, \mathbf{z}). \quad (6)$$

For a single time series $\mathbf{y} = \{y_t\}_{t=1}^T$ the ELBO is given by, $\mathcal{L}_{\phi,\theta,\gamma}^{\text{KVAE}}$

$$\mathcal{L}_{\phi,\theta,\gamma}^{\text{KVAE}} = \mathbb{E}_{q_{\phi}(\mathbf{x} \mid \mathbf{y})} \left[\log \frac{p_{\theta}(\mathbf{y} \mid \mathbf{x})}{q_{\phi}(\mathbf{x} \mid \mathbf{y})} \right] + \mathbb{E}_{p_{\gamma}(\mathbf{z} \mid \mathbf{x})} \left[\log \frac{p_{\gamma}(\mathbf{x}, \mathbf{z})}{p_{\gamma}(\mathbf{z} \mid \mathbf{x})} \right], \quad (7)$$

where ϕ and θ are the encoder and decoder parameters, respectively, and $\gamma = \{A, C, R, Q, \mu_1, P_1\}$ are the LG-SSM parameters. It is possible to sample $(\tilde{\mathbf{x}}, \tilde{\mathbf{z}})$ by first sampling $\tilde{\mathbf{x}} \sim q_{\theta}(\mathbf{x} \mid \mathbf{y})$ and then conditionally sampling $\tilde{\mathbf{z}} \sim p_{\gamma}(\mathbf{z} \mid \tilde{\mathbf{x}})$. Notice that $p_{\gamma}(\mathbf{z} \mid \tilde{\mathbf{x}})$ is tractable using the Kalman smoother algorithm and the joint distribution $p_{\gamma}(\mathbf{x}, \mathbf{z})$ is given by (4). With the re-parameterization trick [21] the model can be trained end-to-end to minimize the negative ELBO using e.g. stochastic gradient descent.

3 Method

Unlike a standard Kalman VAE, our method operates in image *transformations* and not image per se. More specifically, we assume that the images \mathbf{y} are observations from the dynamical state-space model

$$\begin{aligned} \varphi_t &= f(\varphi_{t-1}) + \epsilon_t, \\ y_t &= g(\varphi_t, y_M) + \eta_t, \end{aligned} \quad (8)$$

where $y_M \in \mathcal{M}$ is a reference image, φ_t is the image transformation from the stationary image domain to the image domain at time t and ϵ_t, η_t are process and measurement noise, respectively. We hereby describe the model as a sequence of spatiotemporal image registrations. To be consistent with the medical image community we define y_M as the moving image. An illustration and graphical representation of our model are provided in Figure 1.

The dynamics of our model are driven by the transformation φ_t with respect to the spatial information in y_M . To include the spatial information of y_M we

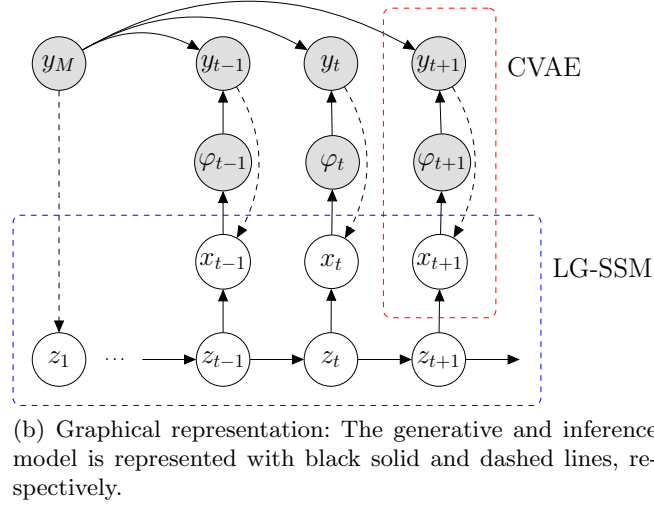
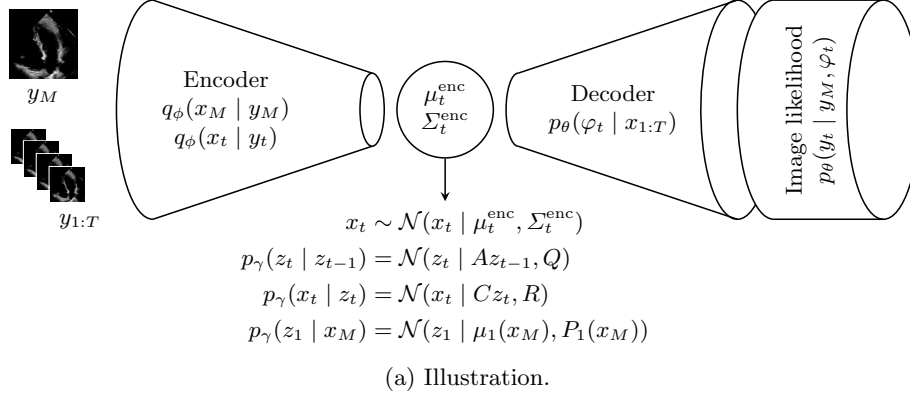


Fig. 1: Illustration (a) and graphical representation (b) of our model. Similar to a Kalman VAE, we learn a lower-dimensional linear-Gaussian state-space model from data, but unlike a Kalman VAE our model operates on image transformations φ_t and not images.

have used a modified Kalman VAE, where the mappings to and from the latent representation are given by a conditional variational auto-encoder (CVAE) [20], conditioned on the moving image y_M . The motion model in the latent space is modeled with an LG-SSM. Spatial information is included in the motion model by condition the initial state prior on the latent representation, x_M of the moving image. The initial prior in the LG-SSM is then given by $p_\gamma(z_1 | x_M) = \mathcal{N}(z_1 | \mu_1(x_M), P_1(x_M))$. For this, we use a fully connected neural network to estimate the mean and variance of this distribution. The parameters of our model can be jointly updated by maximizing the ELBO, $\mathcal{L}_{\phi, \theta, \gamma}$

$$\mathbb{E}_{q_\phi(\mathbf{x}, x_M | \mathbf{y}, y_M)} \left[\log \frac{p_\theta(\mathbf{y} | \mathbf{x}, y_M)}{q_\phi(\mathbf{x}, x_M | \mathbf{y}, y_M)} \right] + \mathbb{E}_{p_\gamma(\mathbf{z} | \mathbf{x}, x_M)} \left[\log \frac{p_\gamma(\mathbf{x}, \mathbf{z} | x_M)}{p_\gamma(\mathbf{z} | \mathbf{x}, x_M)} \right], \quad (9)$$

where the ELBO contains of one VAE-part and one LG-SSM-part. For the VAE-part, the generative model is given by $p_\theta(\mathbf{y} | \mathbf{x}, x_M) = \prod_{t=1}^T p_\theta(y_t | x_t, y_M)$ and the posterior $q_\phi(\mathbf{x}, x_M | \mathbf{y}, y_M) = q_\phi(x_M | y_M) \prod_{t=1}^T q_\phi(x_t | y_t)$. In the LG-SSM part the prior is given by

$$p_\gamma(\mathbf{x}, \mathbf{z} | x_M) = p_\gamma(z_1 | x_M) \prod_{t=1}^T p_\gamma(x_t | z_t) \prod_{t=2}^T p_\gamma(z_t | z_{t-1}) \quad (10)$$

and the exact conditional posterior $p_\gamma(\mathbf{z} | \mathbf{x}, x_M) = \prod_{t=1}^T p_\gamma(z_t | \mathbf{x}, x_M)$ can be obtained with RTS smoothing.

3.1 Likelihood

In the Kalman VAE the likelihood is assumed to come from some parametric family of distributions, parameterized by the decoder network $D_\theta(x_t)$. Instead of modeling the likelihood of the image intensity we model the motion, i.e. the likelihood of the image transformation φ_t . From the decoder this is modeled

$$p_\theta(\varphi_t | x_t) = \mathcal{N}(\varphi_t | \mu_t^{\text{dec}}, \Sigma_t^{\text{dec}}), \quad (11)$$

as a multivariate Gaussian distribution, i.e. the decoder outputs μ_t^{dec} and Σ_t^{dec} . A common disadvantage of image-based VAEs is blurry reconstructions due to the restrictive assumption of a Gaussian likelihood [9]. High frequencies, like sharp edges and fine details in the images are often missed in the reconstructions [7]. In the space of image transformations, on the other hand, Gaussian assumptions are quite reasonable. Existing methods use Gaussian kernels to regularize the displacement field and avoid improbable transformations [37]. We then estimate the image likelihood as a noisy observation of the transformed image, $y_M \circ \varphi_t$, i.e.

$$p_\theta(y_t | y_M, \varphi_t) = \mathcal{N}(y_t | y_M \circ \varphi_t, \sigma_t^2 I), \quad (12)$$

for some noise σ_t .

4 Experiments

4.1 Dataset

In our experiments, we used the EchoNet-Dynamic dataset [31]. The dataset consists of 10030 2D ultrasound echocardiogram time series with 112×112 pixel frames. We fixed the time horizon to 50 time steps ($T = 50$), which corresponded to 1 second and approximately included one cardiac cycle. We extracted one sequence per time series with a randomized start position. Sequences shorter than the fixed horizon were removed (315). We allocated 7220 sequences for training, 1237 for testing and 1258 for validation. The image intensity was normalized to $[0, 1]$ for all images.

4.2 Metrics

We evaluate our model using three metrics, the Dice coefficient [8], the percentage of non-positive Jacobians (Jacobian determinants), and the execution time.

The data sequence included human expert segmentation of the left ventricle at two different time points. We used the image for the first human expert segmentation as moving image y_M , and estimated the transformation for the sequence, including the time step for the other human expert segmented image. We can then measure the quality of transformation with the Dice coefficient, the overlap between the human expert segmentation, S_t and our estimation, $S_M \circ \varphi_t$,

$$\text{Dice} = 2 \frac{|S_t \cap (S_M \circ \varphi_t)|}{|S_t| + |S_M \circ \varphi_t|}, \quad (13)$$

where a perfect overlap is indicated with a Dice coefficient of 1, and 0 for no overlap.

The percentage of non-positive elements in the Jacobian is an indicator of how topology-preserving the transformation is, e.g. if $|J_\varphi(p)| > 0$ for all points p the transformation φ is diffeomorphic. The Jacobian, $|J_\varphi|$ is defined by

$$|J_\varphi| = \begin{vmatrix} \frac{\partial \varphi_x}{\partial x} & \frac{\partial \varphi_x}{\partial y} \\ \frac{\partial \varphi_y}{\partial x} & \frac{\partial \varphi_y}{\partial y} \end{vmatrix}. \quad (14)$$

Although the execution time is hardware dependent, we believe it is a relevant metric since we aim for real-time estimates.

4.3 Implementation Details

Encoder The encoder consists of downsampling convolutional levels with 16, 32, 64 and 128 filters respectively, where the feature maps at each level are first

downsampled using a 2-stride convolutional layer followed by a batch normalization [16] and a leaky ReLU [26] activation function. Furthermore, we use two 1-stride convolutional layers with residual connections [15] before the feature map is downsampled to the next level. The output of the last level is flattened and two dense layers are used—one for the mean, $\{\mu_t^{\text{enc}}\}_{t=1}^T$ and one for the variances, $\{(\sigma_t^{\text{enc}})^2\}_{t=1}^T$.

LG-SSM In the LG-SSM we use a dimension of 16 for our observations, $x_t \in \mathbb{R}^{16}$, and 32 for the state space, $z_t \in \mathbb{R}^{32}$. The mean and variance of the initial prior was estimated with a 3 layer fully connected neural network with 16, 16 and 32 units.

Decoder The decoder layers mirror the encoder with the same filter sizes and residual connections at each level. We let the decoder estimate μ_t^{dec} , the mean of the transformation likelihood, and we used a fixed covariance $\Sigma_t^{\text{dec}} = 0.01^2 I$. When sampling from the transformation likelihood we apply a mask which corresponds to the cone-shaped field-of-view of the ultrasound image.

The mean of the image likelihood is estimated by the sample from the transformation likelihood and applying the transformation on a moving image y_M . For this, we use a spatial transformation module [17, 3]. In this example, we use the first image in the time sequence as a moving image. The variance for the image likelihood was fixed to $\sigma_t^2 = 0.01^2$.

Training The model is trained end-to-end using importance sampling to maximize the ELBO in (9) by jointly updating all parameters $\{\theta, \phi, \gamma\}$ in the model. We use a monotonic annealing schedule weight [11] to the posteriors in the loss function. As an optimizer, we use Adam with exponential decay with factor 0.85 every 20 epochs and an initial learning rate of 10^{-4} . We use a batch size of 4 image time series and train the model for 50 epochs on a single Nvidia GeForce GTX 1080 Ti graphic card (≈ 17 hours training). We have implemented our method into the Tensorflow framework [28] and the code is publicly available ³.

Evaluation When evaluating the result we use samples from the filtered distribution $x_t \sim p_\gamma(x_t | z_{1:t})$. We found that our initial model produced transformations where the Jacobian was frequently negative. We therefore apply regularization to the displacement field using a Gaussian kernel, g_σ

$$\hat{\varphi}_t = \varphi_t \star g_\sigma, \quad (15)$$

as an alternative version of our model.

³ <https://github.com/ngunnar/med-dyn-reg>

4.4 Result

We compare our model with the Demons algorithm [37]. Demons is a popular and fast iterative method for image registration. Since it is iterative, the number of iterations is manually selected. We choose the number of iterations to 40, which gives a fair trade-off between accuracy and computational efficiency in this experiment. We also compare the result with no applied registration to verify the improvements. The average result on the validation data is shown in Table 1.

Model	info	Avg. Dice	\uparrow % $ \mathbf{J}_\varphi \leq 0$ \downarrow	GPU (s) \downarrow	CPU (s) \downarrow
our	filtered	0.81 ± 0.06	$2.7\% \pm 2.7\%$	$0.09 \pm 0.3 \cdot 10^{-2}$	$0.22 \pm 0.5 \cdot 10^{-2}$
our reg	filtered	0.81 ± 0.06	$0.5\% \pm 1.0\%$	$0.09 \pm 0.3 \cdot 10^{-2}$	$0.33 \pm 1 \cdot 10^{-2}$
Demons	40 iter.	0.81 ± 0.07	$1.2\% \pm 1.0\%$	-	$1.64 \pm 2 \cdot 10^{-2}$
None	-	0.74 ± 0.07	-	-	-

Table 1: We compare the average Dice, percentage of negative Jacobian determinants, and execution time with the Demons algorithm. The time is the average execution time for the entire sequence.

Visualization In Figure 2, we show the result of one sequence where we transform both the image and the human expert segmentation from one time step to the other. In this example the Dice coefficient between the other human expert segmentation at time 16: our estimation is 0.732, the Demons algorithm is 0.715, and no registration is 0.583.

Latent analysis From the dynamics in the latent space, we can estimate the filtered, smooth, and predictive distributions. In Figure 3 we show those estimates for one of the latent space dimensions given three examples of input data: all observed values are known, imputation with every 3th sample observed, and extrapolation for the last 5. We here observed a continuous curve from where it is possible to impute and extrapolate for missing values.

Extrapolating image sequence The model is generative — given a moving image, y_M we can generate a displacement field by sampling from the initial prior in the latent space and propagating this sample forward in time. Figure 4 illustrates the generated result for one sample.

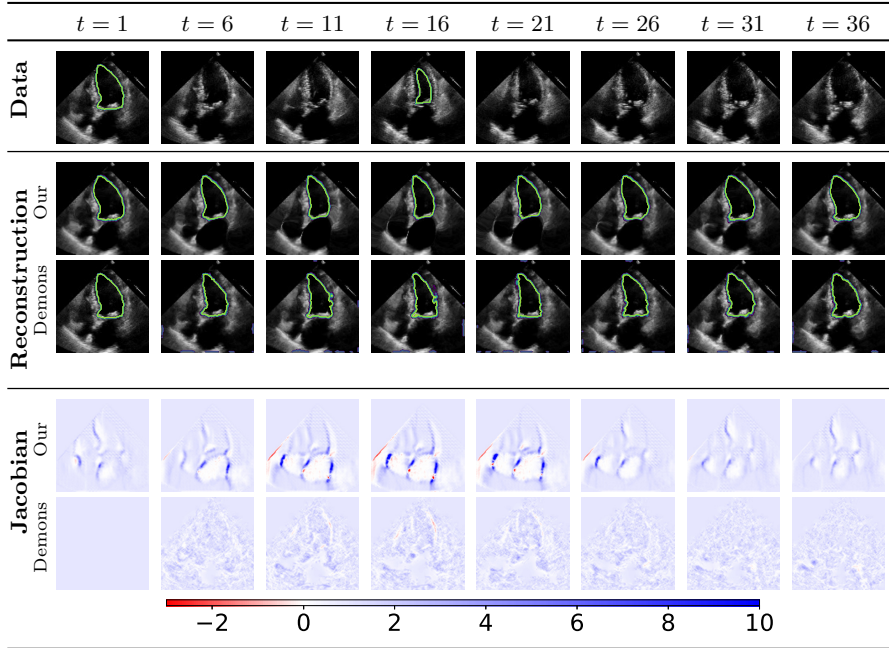


Fig. 2: Reconstructions and Jacobians for a single time sequence using our model and the Demons algorithm. We transfer a segmented region from time point, $t = 1$ to the other in the sequence. In this example, the Dice coefficient between the human expert segmentation at $t = 16$ and our estimate is 0.732. The Dice coefficient using Demons algorithm is 0.715.

5 Discussion

We have described an unsupervised method for extracting latent linear dynamics directly from a medical image time series and show how we can reconstruct the displacement field from the lower-dimensional latent linear dynamic system. With a similar performance in Dice score, our model outperformed the conventional method in speed.

We also illustrate how we can impute missing samples and extrapolate forward in time. Extrapolation support is beneficial for real-time systems when action must be taken given observed data. Good estimates of future states may be necessary to compensate for the system latency. This has e.g. been investigated for the case of real-time adaptive radiotherapy where latency in the motion feedback loop has been seen to cause a decrease in the quality of the treatment [4].

However, we also verified implausible transformation vectors, i.e., Jacobian determinants with non-positive values. Those values mostly appear in regions of the images where the intensity is zero (67%). This is not surprising since we do not handle the regularization of the displacement field directly in the

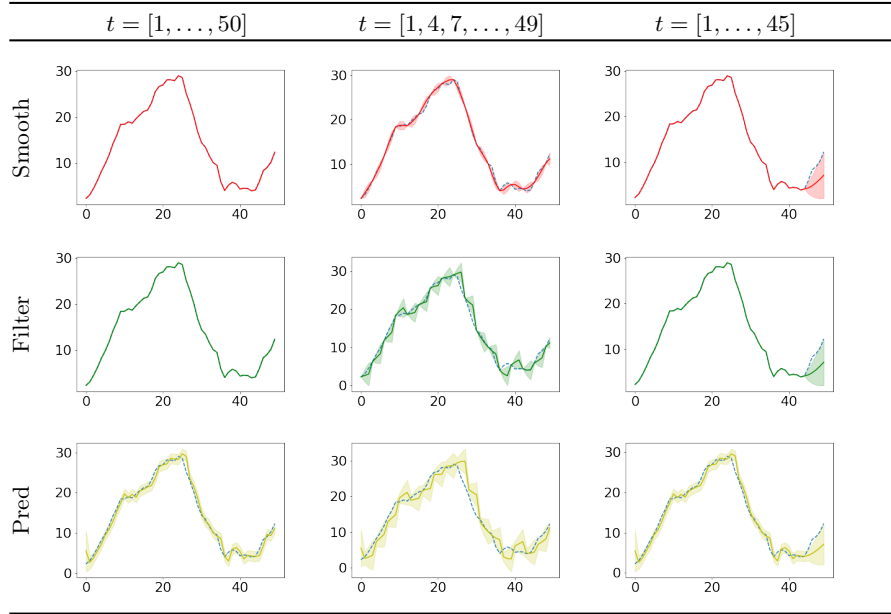


Fig. 3: Distributions of the smooth, filtered, and one-step prediction distribution given observed data for one of the 16 dimensions in the latent observation space. The blue dashed lines are the observed latent variable for the entire sequence, the distributions are represented by their average (solid line), and standard deviation (shaded region).

model. We showed that a low-pass Gaussian filter reduces the number of non-negative Jacobian determinants without significantly affecting performance. We estimate the transformation likelihood as an independent Gaussian with fixed variance which is probably a too strong assumption. More likely, the intensities of nearby pixels are correlated, which could be captured for instance by having a Laplacian structured precision matrix. We believe a richer explanation of the transformation likelihood could address this better, and also provide a better uncertainty estimation of the image transformation. Another approach to regularize the transformation could be to estimate a sparse representation of the displacement field and use interpolation techniques [13], like B-splines [34] or thin plate splines [6] to estimate the dense representation. Furthermore, diffeomorphic deformations can be enforced by applying exponential layers [24] to the network.

In our experiment, we estimated the 2D dynamics based on 2D echocardiogram time series. As further work, we want to extend this to the complete 3D motion.

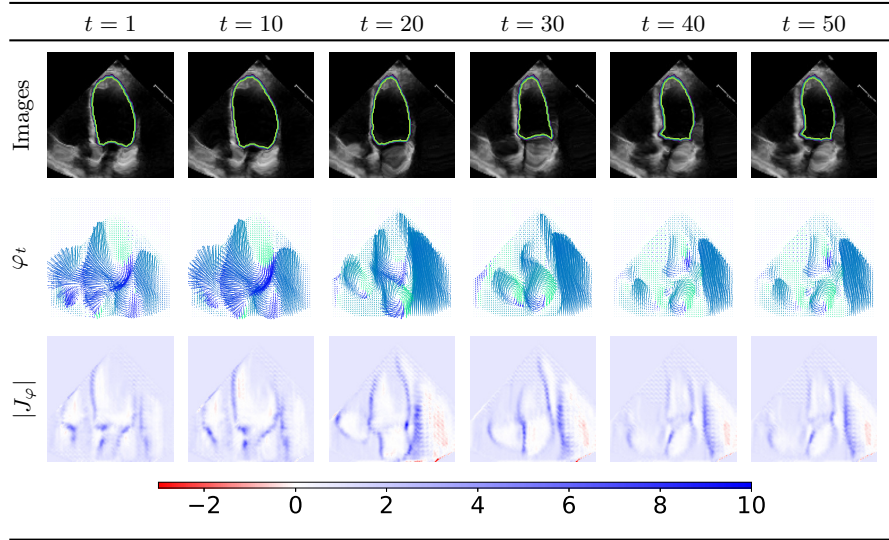


Fig. 4: Generated transformations by sampling an initial position in the latent space. Here we show the transformed moving image (top), the displacement field (middle) and the Jacobian of the generated data (bottom).

Acknowledgement

This research was supported by *Wallenberg AI, Autonomous Systems and Software Program (WASP)* funded by Knut and Alice Wallenberg Foundation, and the Swedish Foundation for Strategic Research grant SM19-0029.

References

- [1] Elsa D Angelini, Andrew F Laine, Shin Takuma, Jeffrey W Holmes, and Shunichi Homma. “LV volume quantification via spatiotemporal analysis of real-time 3-D echocardiography”. In: *IEEE transactions on medical imaging* 20.6 (2001), pp. 457–469.
- [2] Shaojie Bai, J Zico Kolter, and Vladlen Koltun. “An empirical evaluation of generic convolutional and recurrent networks for sequence modeling”. In: *arXiv preprint arXiv:1803.01271* (2018).
- [3] Guha Balakrishnan, Amy Zhao, Mert Sabuncu, John Guttag, and Adrian V. Dalca. “VoxelMorph: A Learning Framework for Deformable Medical Image Registration”. In: *IEEE TMI: Transactions on Medical Imaging* 38 (8 2019), pp. 1788–1800.

- [4] James L Bedford, Martin F Fast, Simeon Nill, Fiona MA McDonald, Merina Ahmed, Vibeke N Hansen, and Uwe Oelfke. “Effect of MLC tracking latency on conformal volumetric modulated arc therapy (VMAT) plans in 4D stereotactic lung treatment”. In: *Radiotherapy and Oncology* 117.3 (2015), pp. 491–495.
- [5] Roberto T Blanco, Risto Ojala, Juho Kariniemi, Jukka Perälä, Jaakko Niinimäki, and Osmo Tervonen. “Interventional and intraoperative MRI at low field scanner—a review”. In: *European journal of radiology* 56.2 (2005), pp. 130–142.
- [6] Fred L Bookstein. “Thin-plate splines and the atlas problem for biomedical images”. In: *Biennial International Conference on Information Processing in Medical Imaging*. Springer. 1991, pp. 326–342.
- [7] Lei Cai, Hongyang Gao, and Shuiwang Ji. “Multi-stage variational auto-encoders for coarse-to-fine image generation”. In: *Proceedings of the 2019 SIAM International Conference on Data Mining*. SIAM. 2019, pp. 630–638.
- [8] Lee R Dice. “Measures of the amount of ecologic association between species”. In: *Ecology* 26.3 (1945), pp. 297–302.
- [9] Alexey Dosovitskiy and Thomas Brox. “Generating images with perceptual similarity metrics based on deep networks”. In: *Advances in neural information processing systems* 29 (2016), pp. 658–666.
- [10] Marco Fraccaro, Simon Kamronn, Ulrich Paquet, and Ole Winther. “A disentangled recognition and nonlinear dynamics model for unsupervised learning”. In: *Advances in Neural Information Processing Systems*. 2017, pp. 3601–3610.
- [11] Hao Fu, Chunyuan Li, Xiaodong Liu, Jianfeng Gao, Asli Celikyilmaz, and Lawrence Carin. “Cyclical Annealing Schedule: A Simple Approach to Mitigating KL Vanishing”. In: *NAACL*. 2019.
- [12] Niklas Gunnarsson, Jens Sjölund, Peter Kimstrand, and Thomas B Schön. “Unsupervised dynamic modeling of medical image transformations”. In: *2022 25th International Conference on Information Fusion (FUSION)*. IEEE. 2022, pp. 01–07.
- [13] Niklas Gunnarsson, Jens Sjölund, and Thomas B. Schön. “Registration by tracking for sequential 2D MRI”. In: *arXiv preprint arXiv:2003.10819* (2020).
- [14] Danijar Hafner, Timothy Lillicrap, Jimmy Ba, and Mohammad Norouzi. “Dream to Control: Learning Behaviors by Latent Imagination”. In: *arXiv preprint arXiv:1912.01603* (2019).
- [15] Kaiming He, Xiangyu Zhang, Shaoqing Ren, and Jian Sun. “Deep residual learning for image recognition”. In: *Proceedings of the IEEE conference on computer vision and pattern recognition*. 2016, pp. 770–778.
- [16] Sergey Ioffe and Christian Szegedy. “Batch normalization: Accelerating deep network training by reducing internal covariate shift”. In: *International conference on machine learning*. PMLR. 2015, pp. 448–456.

- [17] Max Jaderberg, Karen Simonyan, Andrew Zisserman, et al. “Spatial transformer networks”. In: *Advances in neural information processing systems* 28 (2015), pp. 2017–2025.
- [18] Rudolph Emil Kalman. “A new approach to linear filtering and prediction problems”. In: *Journal of basic Engineering* 82.1 (1960), pp. 35–45.
- [19] Maximilian Karl, Maximilian Soelch, Justin Bayer, and Patrick Van der Smagt. “Deep variational Bayes filters: Unsupervised learning of state space models from raw data”. In: *arXiv preprint arXiv:1605.06432* (2016).
- [20] Diederik P Kingma, Shakir Mohamed, Danilo Jimenez Rezende, and Max Welling. “Semi-supervised learning with deep generative models”. In: *Advances in neural information processing systems*. 2014, pp. 3581–3589.
- [21] Diederik P Kingma and Max Welling. “Auto-Encoding Variational Bayes”. In: *ICLR* (2014).
- [22] Mark A Kramer. “Nonlinear principal component analysis using autoassociative neural networks”. In: *AIChE journal* 37.2 (1991), pp. 233–243.
- [23] Julian Krebs, Hervé Delingette, Nicholas Ayache, and Tommaso Mansi. “Learning a Generative Motion Model from Image Sequences based on a Latent Motion Matrix”. In: *IEEE Transactions on Medical Imaging* 40.5 (2021), pp. 1405–1416.
- [24] Julian Krebs, Hervé Delingette, Boris Maillhé, Nicholas Ayache, and Tommaso Mansi. “Learning a probabilistic model for diffeomorphic registration”. In: *IEEE transactions on medical imaging* 38.9 (2019), pp. 2165–2176.
- [25] Rahul Krishnan, Uri Shalit, and David Sontag. “Structured inference networks for nonlinear state space models”. In: *Proceedings of the AAAI Conference on Artificial Intelligence*. Vol. 31. 2017.
- [26] Andrew L Maas, Awni Y Hannun, and Andrew Y Ng. “Rectifier nonlinearities improve neural network acoustic models”. In: *Proc. icml*. Vol. 30. Citeseer. 2013, p. 3.
- [27] Michael Markl, Alex Frydrychowicz, Sebastian Kozerke, Mike Hope, and Oliver Wieben. “4D flow MRI”. In: *Journal of Magnetic Resonance Imaging* 36.5 (2012), pp. 1015–1036.
- [28] Martín Abadi, Ashish Agarwal, Paul Barham, Eugene Brevdo, Zhifeng Chen, Craig Citro, Greg S. Corrado, Andy Davis, Jeffrey Dean, Matthieu Devin, Sanjay Ghemawat, Ian Goodfellow, Andrew Harp, Geoffrey Irving, Michael Isard, Yangqing Jia, Rafal Jozefowicz, Lukasz Kaiser, Manjunath Kudlur, Josh Levenberg, Dandelion Mané, Rajat Monga, Sherry Moore, Derek Murray, Chris Olah, Mike Schuster, Jonathon Shlens, Benoit Steiner, Ilya Sutskever, Kunal Talwar, Paul Tucker, Vincent Vanhoucke, Vijay Vasudevan, Fernanda Viégas, Oriol Vinyals, Pete Warden, Martin Wattenberg, Martin Wicke, Yuan Yu, and Xiaoqiang Zheng. *TensorFlow: Large-Scale Machine Learning on Heterogeneous Systems*. Software available from tensorflow.org. 2015. URL: <https://www.tensorflow.org/>.

- [29] Jamie R McClelland, David J Hawkes, Tobias Schaeffter, and Andrew P King. “Respiratory motion models: a review”. In: *Medical image analysis* 17.1 (2013), pp. 19–42.
- [30] Kathryn Mittauer, Bhudatt Paliwal, Patrick Hill, John E Bayouth, Mark W Geurts, Andrew M Baschnagel, Kristin A Bradley, Paul M Harari, Stephen Rosenberg, Jeffrey V Brower, et al. “A new era of image guidance with magnetic resonance-guided radiation therapy for abdominal and thoracic malignancies”. In: *Cureus* 10.4 (2018).
- [31] David Ouyang, Bryan He, Amirata Ghorbani, Neal Yuan, Joseph Ebinger, Curtis P Langlotz, Paul A Heidenreich, Robert A Harrington, David H Liang, Euan A Ashley, et al. “Video-based AI for beat-to-beat assessment of cardiac function”. In: *Nature* 580.7802 (2020), pp. 252–256.
- [32] Tinsu Pan, Ting-Yim Lee, Eike Rietzel, and George TY Chen. “4D-CT imaging of a volume influenced by respiratory motion on multi-slice CT”. In: *Medical physics* 31.2 (2004), pp. 333–340.
- [33] Herbert E Rauch, F Tung, and Charlotte T Striebel. “Maximum likelihood estimates of linear dynamic systems”. In: *AIAA journal* 3.8 (1965), pp. 1445–1450.
- [34] Daniel Rueckert, Luke I Sonoda, Carmel Hayes, Derek LG Hill, Martin O Leach, and David J Hawkes. “Nonrigid registration using free-form deformations: application to breast MR images”. In: *IEEE transactions on medical imaging* 18.8 (1999), pp. 712–721.
- [35] Vaibhav Saxena, Jimmy Ba, and Danijar Hafner. “Clockwork Variational Autoencoders”. In: *arXiv preprint arXiv:2102.09532* (2021).
- [36] Kavitha Srinivasan, Mohammad Mohammadi, and Justin Shepherd. “Applications of linac-mounted kilovoltage Cone-beam Computed Tomography in modern radiation therapy: A review”. In: *Polish journal of radiology* 79 (2014), p. 181.
- [37] J-P Thirion. “Image matching as a diffusion process: an analogy with Maxwell’s demons”. In: *Medical image analysis* 2.3 (1998), pp. 243–260.
- [38] Poonam Verma, Huanmei Wu, Mark Langer, Indra Das, and George Sandison. “Survey: real-time tumor motion prediction for image-guided radiation treatment”. In: *Computing in Science & Engineering* 13.5 (2010), pp. 24–35.
- [39] Jacob Walker, Ali Razavi, and Aäron van den Oord. “Predicting video with VQVAE”. In: *arXiv preprint arXiv:2103.01950* (2021).
- [40] Michael J Wallace, Michael D Kuo, Craig Glaiberman, Christoph A Binkert, Robert C Orth, Gilles Soulez, Technology Assessment Committee of the Society of Interventional Radiology, et al. “Three-dimensional C-arm cone-beam CT: applications in the interventional suite”. In: *Journal of Vascular and Interventional Radiology* 19.6 (2008), pp. 799–813.
- [41] Yoram A Weil, Meir Liebergall, Rami Mosheiff, David L Helfet, and Andrew D Pearle. “Long bone fracture reduction using a fluoroscopy-based navigation system: a feasibility and accuracy study”. In: *Computer Aided Surgery* 12.5 (2007), pp. 295–302.